ISSN 0021-3640, JETP Letters, 2014, Vol. 99, No. 12, pp. 706–711. © Pleiades Publishing, Inc., 2014.
Original Russian Text © M.S. Platunov, S.N. Varnakov, S.M. Zharkov, G.V. Bondarenko, E. Weschke, E. Schierle, S.G. Ovchinnikov, 2014, published in Pis'ma v Zhurnal Eksperimental'noi i Teoreticheskoi Fiziki, 2014, Vol. 99, No. 12, pp. 817–823.

Analysis of the Structure and Magnetic Properties of an Interface in Multilayered $(Fe/Si)_N$ Nanostructures with the Surface-Sensitive XMCD Method

M. S. Platunov[a–c], S. N. Varnakov[a, c], S. M. Zharkov[a, b], G. V. Bondarenko[a], E. Weschke[d], E. Schierle[d], and S. G. Ovchinnikov[a–c]

[a] *Kirensky Institute of Physics, Siberian Branch, Russian Academy of Sciences, Akademgorodok, Krasnoyarsk, 660036 Russia*
e-mail: platunov@iph.krasn.ru
[b] *Siberian Federal University, pr. Svobodnyi 79, Krasnoyarsk, 660041 Russia*
[c] *Siberian State Aerospace University, pr. Gazety Krasnoyarskii Rabochii, Krasnoyarsk, 660014 Russia*
[d] *BESSY II, Helmholtz-Zentrum Berlin, 12489 Berlin, Germany*

Received May 19, 2014

The structural and magnetic properties of $(Fe/Si)_N$ nanostructures obtained by successive deposition on the SiO_2/Si(100) surface at a temperature of the substrate of 300 K have been studied. The thicknesses of all Fe and Si layers have been determined by transmission electron microscopy measurements. The magnetic properties have been studied by the X-ray magnetic circular dichroism (XMCD) method near the Fe $L_{3,2}$ absorption edges. The orbital (m_l) and spin (m_S) contributions to the total magnetic moment of iron have been separated. The thicknesses of magnetic and nonmagnetic iron silicide on the Si/Fe and Fe/Si interfaces have been determined with the surface sensitivity of the XMCD method and the model of the interface between the nonmagnetic and weakened magnetic phases.

DOI: 10.1134/S002136401412011X

1. INTRODUCTION

Since silicides of 3*d* metals have a rich variety of physical properties, they are of significant fundamental and applied interest [1]. A silicide is formed through the penetration of an atom of one type to the lattice of other atoms. The formation of silicides strongly depends on the crystal quality of multilayers, in particular, on the roughness of an interface [2]. The structure of the ferromagnetic interface is a key parameter in the fabrication of magnetic multilayer structures exhibiting the giant magnetoresistance effect.

The formation of iron silicides on an interface in the case where Fe is deposited on Si differs from the case where Si is deposited on Fe [3–7]. In particular, Kläges et al. [3] stated that the Si/Fe interface obtained by depositing Si on Fe contains several nonmagnetic phases of different compositions. Strijkers et al. [4] reported that crystalline iron silicide, which is determined as the c-$Fe_{1-x}Si_x$ phase with the solid solution of ferromagnetic silicide, is formed at the Si/Fe interface. The thicknesses and roughnesses of interfaces of nonmagnetic Fe/Si structures were determined by different methods. In particular, it was shown in [5–7] that both the thickness, 1.3–1.4 nm, and roughness, 0.5–0.6 nm, of an interface are independent of the thicknesses of Fe and Si layers, as well as the method of fabrication and growth rates.

Although numerous data were reported, the distribution of magnetic and nonmagnetic silicides in Si/Fe and Fe/Si interfaces is still unclear. In this work, we analyze the spatial structure of an interface with the use of the surface sensitive method of X-ray magnetic circular dichroism (XMCD). Complex study of structural and local magnetic properties of Fe/Si nanolayers is performed. The relative amount of the magnetic phase that is formed at Si/Fe and Fe/Si interfaces is the object of investigation.

2. SAMPLES AND EXPERIMENTAL PROCEDURE

Two $(Si/Fe)_3/SiO_2/Si(100)$ samples with different thicknesses of Fe and different packing of ^{57}Fe isotope (nos. 1 and 2) were obtained by means of thermal evaporation in ultrahigh vacuum (base pressure $P = 10^{-8}$ Pa) at room temperature with the use of the modernized molecular beam facility Angara [8]. The ^{57}Fe isotope was added to the structure for studying the morphology and chemical composition of various Si/Fe and Fe/Si interfaces by the conversion electron Mössbauer spectroscopy method [6]. Magnetic structures were produced by successive deposition of Fe and

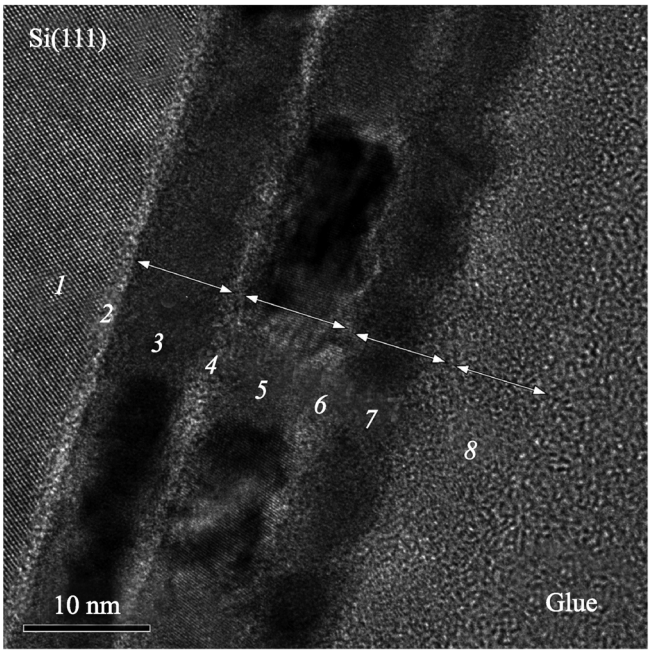

Fig. 1. Electron microscopy image of the cross section of Fe/Si structures (sample no. 2).

Si layers on the prepared Si(100) surface with a thin SiO_2 buffer layer. The growth rate was controlled in situ by a high-speed laser ellipsometer. The thicknesses of Fe layers were additionally controlled by means of the X-ray fluorescence method. Structural perfection was determined ex situ by transmission electron microscopy with a JEOL JEM-2100 microscope (Shared Usage Center, Siberian Federal University) [9, 10]. X-ray absorption spectra at the Fe $L_{3,2}$ absorption edges were measured at the UE46-PGM1 beamline of the BESSY II synchrotron at the Helmholtz-Zentrum Berlin. A helical undulator was used as a source of polarized radiation. A planar grating monochromator was used. Measurements were performed at temperatures of 5 and 300 K in a magnetic field of up to 6 T induced by a superconducting magnet. Spectra were recorded in the total electron yield regime [11, 12] because of its surface sensitivity.

Table 1. Thicknesses of the layers according to the transmission electron microscopy study of sample nos. 1 and 2

Sample no. 1	t, nm	Sample no. 2	t, nm
Si	9.8	Si	8.7
Fe	9.8	Fe	7.3
Si	1.1	Si	1.5
Fe	10.5	Fe	8.4
Si	1.1	Si	1.1
Fe	9.5	Fe	8.0
Si/SiO_2	1.5	Si/SiO_2	1.1
Si(100)		Si(100)	
$\sum$Fe	29.8	$\sum$Fe	23.7

The depth of the yield of secondary photoelectrons guarantees that the recorded spectra are determined primarily by Fe atoms near the phase interface. The diameter of the spot at the measurement of an AMCD signal was no less than 200 m. The orientation of the magnetic field or polarization of radiation was changed after each measurement of the spectrum. Self-absorption and saturation effects can influence the spectral weight of near-edge features, introducing errors in the determination of spin and orbital magnetic moments [13]. In view of this circumstance [14], the geometry of the experiment was chosen such that the directions of the magnetic field and incident radiation were perpendicular to the surface of the sample. In this configuration, magnetic saturation for all samples was achieved in a field of 2 T.

In order to apply sum rules [15, 16] to the measured XMCD data, the contribution of photoelectron excitations to continuum states was separated from the absorption cross section with the use of a step function [17, 18]. The intra-atomic dipole term $_T$, which appears in the experimentally determined effective spin magnetic moment $_{S\,\mathrm{eff}} = _S + 7\ _T$, is assumed to be insignificant for the cubic structure of silicide [19]. However, since $_T$ does not vanish completely, spin magnetic moments extracted from experimental data should be treated as effective.

3. EXPERIMENTAL RESULTS AND DISCUSSION

Figure 1 shows the electron microscopy image of the cross section of sample no. 2. According to transmission electron microscopy images, films have a pronounced layered structure including amorphous silicon oxide layers and thin polycrystalline iron layers where the minimum dimension of a crystallite is comparable to the thickness of the film. Smooth variation in the optical contrast is due to gradual change in the atomic concentrations of Fe and Si from layer to layer because of mutual diffusion and subsequent formation of silicides. Table 1 presents the approximated thicknesses for two samples.

In addition, the conversion electron Mössbauer spectroscopy results [6] for sample no. 1 from the same series show the presence of the -Fe sextet and a paramagnetic contribution (broad doublet), which is due to the epitaxially stable nonequilibrium phase (c-FeSi). The simultaneous presence of paramagnetic and ferromagnetic components in conversion electron Mössbauer spectra of Fe/Si structures indicates that these interfaces with a relatively large roughness consist of a spatially distributed environment of Fe from c-$Fe_{1-x}Si_x$ to Fe atoms with the absence of or a few Si atoms as the nearest neighbors. The transformation of

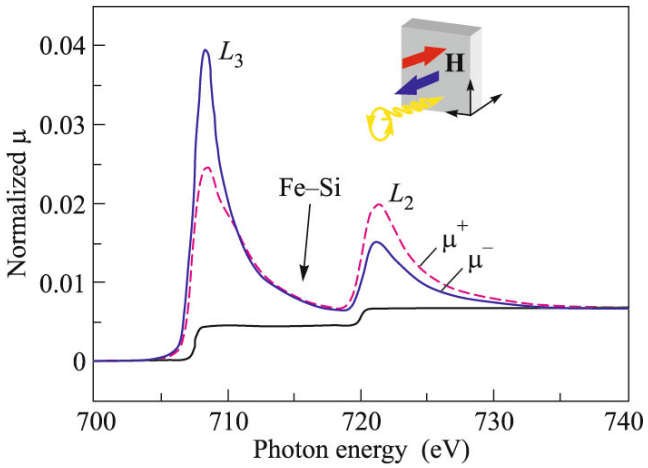

Fig. 2. (Color online) Normalized surface sensitive X-ray absorption spectra (recorded in the total electron yield regime) at the Fe $L_{3,2}$ edges of sample no. 1 at 5 K in a magnetic field of 6 T. The external magnetic field was parallel to the X-ray beam. The black solid line is the step function.

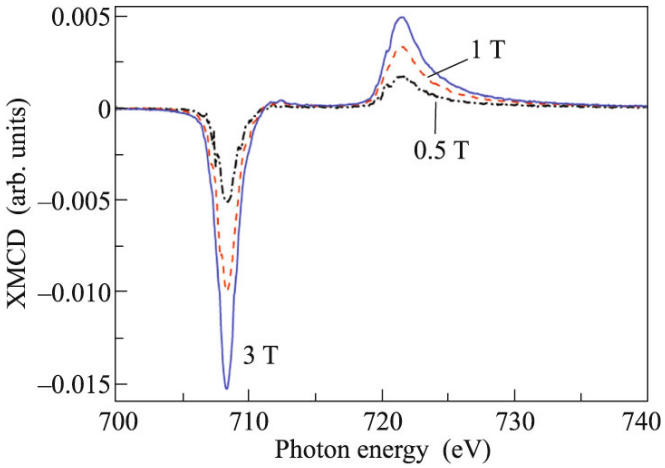

Fig. 3. (Color online) X-ray magnetic circular dichroism spectra of sample no. 1 at 5 K. Lines for $H = 4.5$ and 6 T hardly differ from the line for $H = 3$ T.

a part of Fe/Si interface to the nonmagnetic *c*-FeSi phase should reduce the total saturation magnetization of the samples, which can be quantitatively expressed as a deficit of the magnetic moment of iron [3]. We emphasize that Mössbauer spectroscopy gives volume information, in contrast to XMCD.

Since the experimental X-ray absorption and XMCD spectra are similar for the two samples under study, we discuss only spectra for sample no. 1.

Figures 2 and 3 show normalized X-ray absorption and XMCD spectra, respectively, recorded at a temperature of 5 K in a magnetic field of up to 6 T. The shape of the X-ray absorption spectra at the $L_{3,2}$ edges (Fig. 2) indicates *d*(Fe)/*sp*(Si) hybridization [19, 20]. A barely noticeable shoulder at 715 eV on X-ray absorption spectra indicates the presence of the silicide Fe–Si phase (Fig. 2) [19].

Analysis of the XMCD signal at the Fe $L_{3,2}$ edges shows that the profile and asymptotic behavior of the signal do not change when the temperature is reduced from 300 to 5 K. The maximum XMCD effect is observed in a field of 2–3 T and does not increase with the magnetic field, indicating the saturation of the magnetic moment (Fig. 3).

The total magnetic moment can be separated into the spin, m_S, and orbital, m_l, components with the use of sum rules [15, 16]. The experimental results show that the total magnetic moments per Fe atom for sample nos. 1 and 2 are $M_1 = 1.92$ $_B$ and $M_2 = 1.89$ $_B$, respectively. The magnetic moments obtained in the saturated state are in agreement with the data from other works (see Table 2). The processing of XMCD spectra indicates also that the spin magnetic moment is saturated near 2.5 T for both samples (Figs. 4a and 4b).

The resulting moment of Fe is much smaller than that in bulk -Fe (2.227 $_B$ [21]) and is in good agreement with previously reported values (see Table 2). It is noteworthy that the magnetic moments at the Fe_I and Fe_{II} positions in the Fe_3Si ($D0_3$) structure [24] are 2.2–2.4 $_B$ and 1.35 $_B$, respectively. This corresponds to the average moment 1.775–1.875 $_B$ at the $Fe_{I,II}$ positions, which is in agreement with the results of this work. Consequently, magnetic silicide on the surface in our case is predominantly Fe_3Si.

We emphasize that the orbital magnetic moment is nonzero (Fig. 4). The direction of $\mathbf{m}_{orb}$ is the same as that for the spin moment $\mathbf{m}_{spin}$. According to reported data, the ratio m_{orb}/m_{spin} depends on the atomic structure, dimension, and coordination number. The m_{orb} value in nanostructures is very sensitive to the nearest environment and increases rapidly with a decrease in the coordination number [25].

Table 2. Orbital and spin magnetic moments of sample nos. 1 and 2 in comparison with previously reported data

Reference	m_S, μ_B	m_l, μ_B	$m_S + m_l$, μ_B
bcc Fe [22]	2.36	0.071	2.431
bcc Fe [21]	–	–	2.227
ML Fe [23]	2.31	0.30	2.61
ML Fe [17]	1.98	0.086	2.066
Fe_3Si [19]	1.76 ± 0.1	0.073 ± 0.01	1.833
Sample no. 1	1.71 (300 K)	0.04 (300 K)	1.75
	1.86 (5 K)	0.06 (5 K)	**1.92**
Sample no. 2	1.72 (300 K)	0.04 (300 K)	1.76
	1.85 (5 K)	0.04 (5 K)	**1.89**

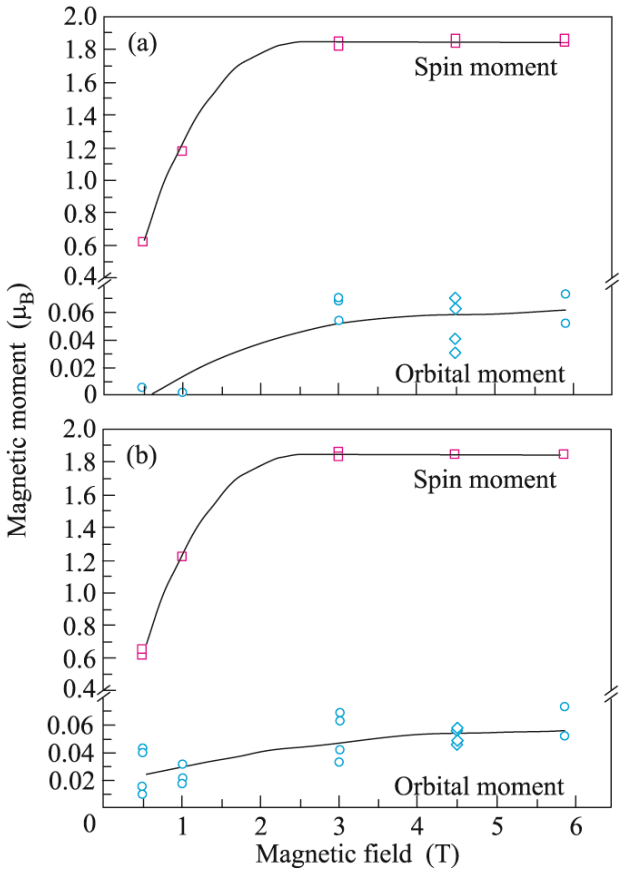

Fig. 4. (Color online) Magnetic-field dependences of the orbital and spin magnetic moments of sample nos. (a) 1 and (b) 2 at 5 K (Fe $L_{3,2}$ absorption edges).

Since the XMCD signal was measured in the total electron yield regime, the total magnetic signal is determined primarily by the upper iron layer and magnetic interface. Furthermore, the XMCD signal is determined primarily by the linear combination of signals from all atoms localized in a sample or silicide. It provides statistical information on silicide in samples.

In measurements of XMCD signals in the total electron yield regime, it is always necessary to estimate the penetration depth of soft X-ray photons. Inaccurate inclusion of this parameter can lead to incorrect interpretation of the magnetic properties of materials under study [17].

The total electron yield is exactly proportional to the absorption cross section if the attenuation length of incident radiation $_x$ is much larger than the electron escape depth $_e$ [12]. In our case, this condition is satisfied at the penetration depth $_x \sim 150$ nm and $_e \sim$ 2.5 nm [17, 19].

In order to describe XMCD data, we introduce a model describing the Si/Fe interface with variable composition by the magnetic profile shown in Fig. 5. We assume that the Si layer is directly followed by the FeSi nonmagnetic silicide layer with the thickness $_1$,

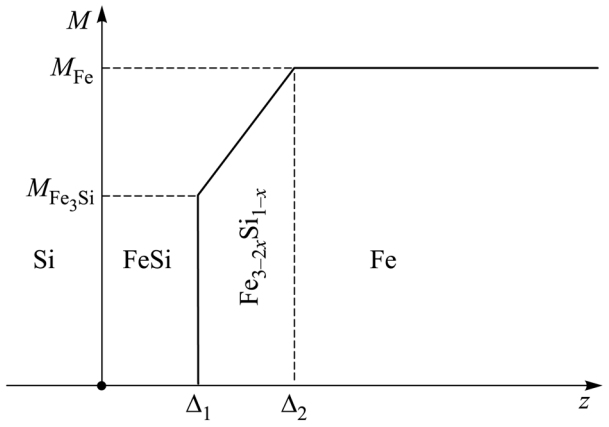

Fig. 5. (Color online) Magnetization profile in the interface with the infinite Fe layer.

which is followed by a continuous series of magnetic solid solutions from Fe_3Si with the magnetization M_{Fe_3Si} to bulk Fe with the magnetization M_{Fe} beginning at the thickness $_2$. For simplicity, we assume a linear increase in the magnetization between M_{Fe_3Si} and M_{Fe}. For the estimate, we take $M_{Fe_3Si} = 1270$ G [26] and $M_{Fe} = 1740$ G. The Fe/Si interface is described by the same model, but with the thicknesses $_2'$ and $_1'$. The models of the magnetic profiles of sample nos. 1 and 2 are shown in Fig. 6. The proposed model can be described by the simple formulas

$$M(z) = \begin{cases} 0 \quad \text{at} \quad 0 \quad z \quad {}_1; \\ M_{Fe_3Si} + M_{Fe} - M_{Fe_3Si} \dfrac{z - {}_1}{{}_2 - {}_1} \\ \text{at} \quad {}_1 \quad z \quad {}_2; \\ M_{Fe} \\ \text{at} \quad {}_2 \quad z \quad d_1 - {}_2'; \\ M_{Fe} - M_{Fe} - M_{Fe_3Si} \dfrac{z - d_1 + {}_2'}{{}_2' - {}_1'} \\ \text{at} \quad d_1 - {}_2' \quad z \quad d_1 - {}_1'; \\ 0 \quad \text{at} \quad d_1 - {}_1' \quad z \quad d_2 + {}_1; \\ M_{Fe_3Si} + M_{Fe} - M_{Fe_3Si} \dfrac{z - d_2 + {}_1}{{}_2 - {}_1} \\ \text{at} \quad d_2 + {}_1 \quad z \quad d_2 + {}_2; \\ M_{Fe} \quad \text{at} \quad d_2 + {}_2 \quad z \quad , \end{cases} \tag{1}$$

where z is the thickness of the film under study; $_1$ and $_2$ are the thickness of the nonmagnetic FeSi layer and the total thickness of the interface, respectively; $d_1 =$

9.8 nm and $d_2 = 10.9$ nm for sample no. 1; and $d_1 =$ 7.3 nm and $d_2 = 8.8$ nm for sample no. 2 (see Table 1).

Taking into account that the number of electrons reaching the surface decreases exponentially as a function of the initial X-ray absorption depth [12], we obtain the equation

$$M = \frac{1}{e}\int M\, z\, e^{-z/\lambda_e} dz = f\left({}_1, {}_2, {}_e \right), \qquad (2)$$

where $_e$ is the electron escape depth. The left-hand side of Eq. (1) contains the measured magnetization $M = m_S + m_l$ for sample nos. 1 and 2 (see Table 2). Integrating M in the indicated limits and solving the equations, we obtain the thicknesses of the nonmagnetic and magnetic layers.

According to [6], the thickness of the silicide layer is $_2 = 1.4$ nm. The thickness of the iron layer of 9.8 nm is fairly large compared to $_e \sim 2.5$ nm for sample no. 1. For this reason, the second interface can be neglected. In this case, the iron layer can be considered as infinite and the model shown in Fig. 5 can be considered instead of the model shown in Fig. 6a.

Then, taking into account that $M_1 = 1.92$ $_B$, Eq. (2) has the form

$$M_1 = e^{-\Delta_1/\lambda_e}\left[M_{Fe_3Si} + \frac{M_{Fe} - M_{Fe_3Si}}{{}_2 - {}_1}\, {}_e \right] - e^{-\Delta_2/\lambda_e}\frac{M_{Fe} - M_{Fe_3Si}}{{}_2 - {}_1}\, {}_e.$$

The solution of this equation for sample no. 1 gives the thicknesses $_1 = 0.23$ nm and $_2 - {}_1 = 1.17$ nm of the nonmagnetic silicide and magnetic layer, respectively.

In the case of sample no. 2, it is necessary to take into account both interfaces from the first iron layer and an additional interface from the second layer (Fig. 6b) whose parameters are the same as for the first layer. According to [7], $'_2 = {}_2/2 = 0.7$ nm. As a result, taking into account the magnetic moment $M_1 = 1.89$ $_B$, the equation describing the magnetic profile of sample no. 2 has the form

$$\begin{aligned} M_2 = M_1 &- e^{-(d_1 - \Delta'_1)/\lambda_e}\left[M_{Fe_3Si} + \frac{M_{Fe} - M_{Fe_3Si}}{{}'_2 - {}'_1}\, {}_e \right] \\ &- e^{-(d_1 - \Delta'_2)/\lambda_e}\frac{M_{Fe} - M_{Fe_3Si}}{{}'_2 - {}'_1}\, {}_e \\ &+ e^{-(d_2 + \Delta_1)/\lambda_e}\left[M_{Fe_3Si} + \frac{M_{Fe} - M_{Fe_3Si}}{{}_2 - {}_1}\, {}_e \right] \\ &- e^{-(d_2 + \Delta_2)/\lambda_e}\frac{M_{Fe} - M_{Fe_3Si}}{{}_2 - {}_1}\, {}_e. \end{aligned} \qquad (3)$$

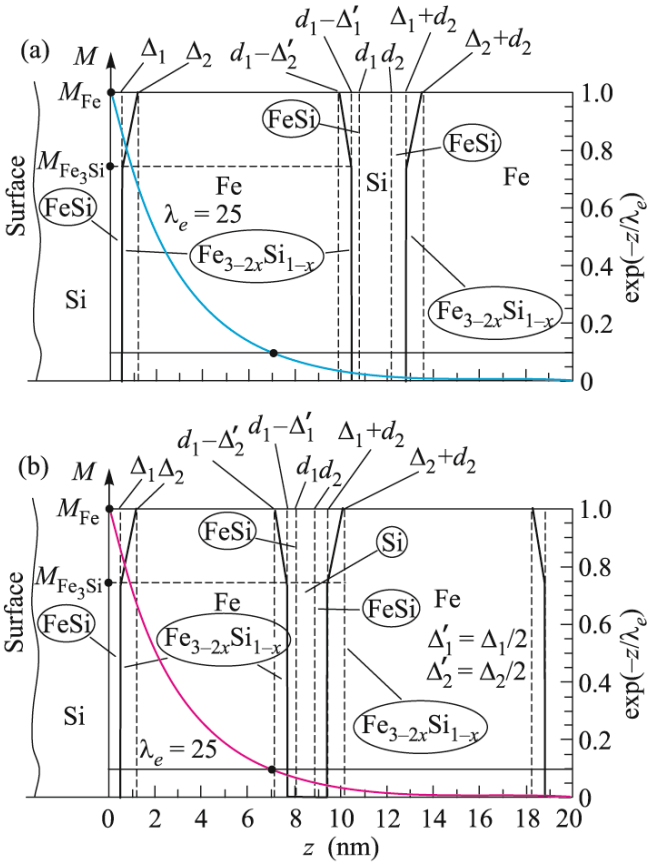

Fig. 6. (Color online) Magnetization profiles in sample nos. (a) 1 and (b) 2 with a decreasing exponential limiting the electron escape depth.

In this case, the thicknesses of the nonmagnetic and magnetic layers in sample no. 2 at $_e \sim 2.5$ nm and $'_2 = 0.7$ nm are $'_1 = 0.15$ nm and $'_2 - {}'_1 =$ 0.55 nm, respectively. Taking into account the error of the proposed model caused by the inaccurate $_e$ value and the difference in the resulting approximated thicknesses of layers for the two samples, the confidence intervals for the thicknesses of magnetic interfaces are 1.1–1.2 and 0.5–0.6 nm for the Si/Fe and Fe/Si interfaces, respectively.

The thicknesses $_2$ and $'_2$ for the Si/Fe and Fe/Si interfaces were taken from [7]. The difference between them can be explained as follows. Iron layers have a crystalline structure. When silicon is deposited on Fe, Si atoms diffuse more easily along the boundaries of Fe grains. In addition, the atomic radius for silicon is smaller than that for iron. Thus, the thicknesses of the interface are larger in the case of the Si/Fe interface. Amorphous silicon limits diffusion of iron to the silicon layer in the case of the Fe/Si interface. Consequently, the interface is thinner in this case.

4. CONCLUSIONS

Transmission electron microscopy studies have shown that the films under study have a layered structure including amorphous Si and SiO_2 layers and polycrystalline Fe layers. Nonmagnetic phases of silicide appear in the process of synthesis of nanostructures.

The thicknesses of the magnetic interfaces obtained from XMCD data are 1.1–1.2 and 0.5–0.6 nm for the Si/Fe and Fe/Si interfaces, respectively. The interface can be represented as $(Fe_3Si)_{1-x} + Fe_x = Fe_{3-2x}Si_{1-x}$.

Thus, we have proposed a method for the determination of the thicknesses of the magnetic and nonmagnetic components of the Fe/Si and Si/Fe interfaces with the use of the elemental and surface sensitivity of the XMCD method.

We are grateful to S.V. Komogortsev for stimulating discussions and to the management of BESSY II, Helmholtz-Zentrum Berlin, for the opportunity of performing experiments at the UE46-PGM1 beamline. This work was supported by the Russian Foundation for Basic Research (project nos. 13-02-01265a and 14-02-31051mol-a), by the Council of the President of the Russian Federation for Support of Young Scientists and Leading Scientific Schools (project no. NSh- 2886.2014.2), by the Presidium of the Russian Academy of Sciences (program no. 24.34), and by the Ministry of Education and Science of the Russian Federation (state contract no. 02.G25.31.0043 and state task for research at Siberian Federal University in 2014).

REFERENCES

1. S. A. Wolf, D. D. Awschalom, R. A. Buhrman, J. M. Daughton, S. von Molnar, M. L. Roukes, and D. M. Treger, Science **294** (5546), 1488 (2001).
2. S. N. Varnakov, S. V. Komogortsev, S. G. Ovchinnikov, J. Bartolomé, and J. Sesé, J. Appl. Phys. **104**, 094703 (2008).
3. R. Kläges, C. Carbone, W. Eberhardt, C. Pampuch, O. Rader, T. Kachel, and W. Gudat, Phys. Rev. B **56**, 10801 (1997).
4. G. J. Strijkers, J. T. Kohlhepp, H. J. M. Swagten, and W. J. M. de Jonge, Phys. Rev. Lett. **84**, 1812 (2000).
5. A. Gupta, D. Kumar, and V. Phatak, Phys. Rev. B **81**, 155402 (2010).
6. L. Badia-Romano, J. Rubin, J. Bartolomé, S. Ovchinnikov, S. Varnakov, C. Magén, J. Rubio-Zuazo, and C. R. Castro, SPIN **4**, 1440002 (2014).
7. S. R. Naik, S. Rai, M. K. Tiwari, and G. S. Lodha, J. Phys. D: Appl. Phys. **41**, 115307 (2008).
8. S. N. Varnakov, A. A. Lepeshev, S. G. Ovchinnikov, A. S. Parshin, M. M. Korshunov, and P. Nevoral, Instrum. Exp. Tech. **47**, 839 (2004).
9. S. M. Zharkov, E. T. Moiseenko, R. R. Altunin, N. S. Nikolaeva, V. S. Zhigalov, and V. G. Myagkov, JETP Lett. **99**, 405 (2014).
10. S. M. Zharkov, R. R. Altunin, E. T. Moiseenko, G. M. Zeer, S. N. Varnakov, and S. G. Ovchinnikov, Solid State Phenom. **215**, 144 (2014).
11. W. Gudat and C. Kunz, Phys. Rev. Lett. **29**, 169 (1972).
12. J. Stöhr, *NEXAFS Spectroscopy* (Springer, Berlin, 1992), Vol. 25.
13. V. Chakarian and Y. U. Idzerda, J. Appl. Phys. **81**, 4709 (1997).
14. R. Nakajima, J. Stöhr, and Y. U. Idzerda, Phys. Rev. B **59**, 6421 (1999).
15. B. T. Thole, P. Carra, F. Sette, and G. van der Laan, Phys. Rev. Lett. **68**, 1943 (1992).
16. P. Carra, B. T. Thole, M. Altarelli, and X. Wang, Phys. Rev. Lett. **70**, 694 (1993).
17. C. T. Chen, Y. U. Idzerda, H. J. Lin, N. V. Smith, G. Meigs, E. Chaban, and F. Sette, Phys. Rev. Lett. **75**, 152 (1995).
18. H. J. Elmers, G. H. Fecher, D. Valdaitsev, S. A. Nepijko, A. Gloskovskii, G. Jakob, and S. Cramm, Phys. Rev. B **67**, 104412 (2003).
19. C. Antoniak, H. C. Herper, Y. N. Zhang, A. Warland, T. Kachel, F. Stromberg, and H. Wende, Phys. Rev. B **85**, 214432 (2012).
20. B. Krumme, C. Weis, H. C. Herper, F. Stromberg, C. Antoniak, A. Warland, and H. Wende, Phys. Rev. B **80**, 144403 (2009).
21. C. Kittel, *Introduction to Solid State Physics*, 6th ed. (Wiley, New York, 1986).
22. C. Piamonteze, P. Miedema, and F. M. de Groot, Phys. Rev. B **80**, 184410 (2009).
23. A. Lehnert, Doctoral Dissertation (Ècole Polytechnique Fèdèrale de Lausanne, 2009).
24. E. G. Moroni, W. Wolf, J. Hafner, and R. Podloucky, Phys. Rev. B **59**, 12860 (1999).
25. J. Bansmann, S. H. Baker, C. Binns, J. A. Blackman, J. P. Bucher, J. Dorantes-Dávila, and Y. Xie, Surf. Sci. Rep. **56**, 189 (2005).
26. H. P. Wijn, *Magnetic Properties of Metals: d-Elements, Alloys and Compounds* (Springer, Berlin, 1991).

Translated by R. Tyapaev